Graphical abstract

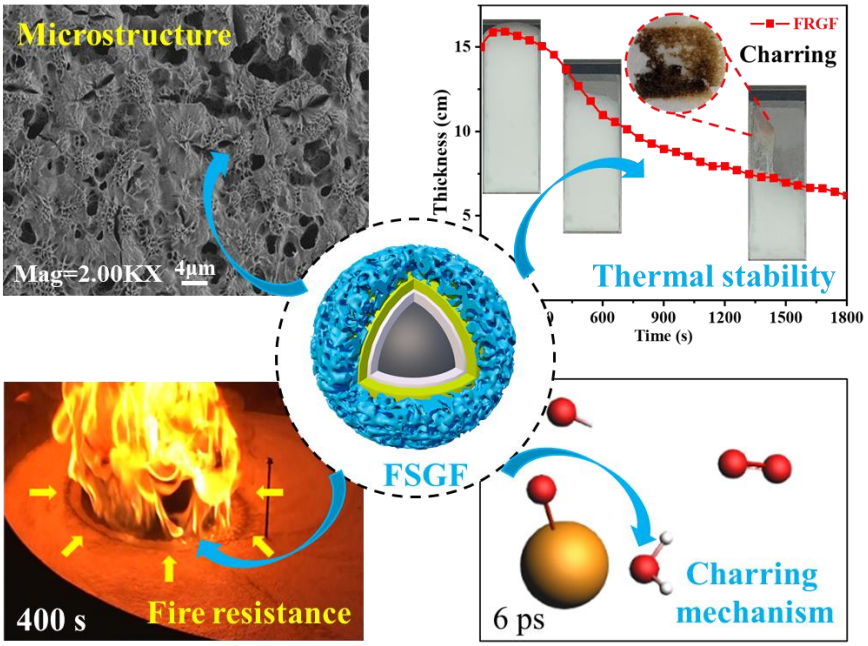

A facile sunflower pectin gel foam for liquid fuel fire suppression with ReaxFF characterisation on its char-enhancing ability

(Tian Chang[a,1], Anthony Chun Yin Yuen[a,1], Zhao Jinlong[b*], Timothy Bo Yuan Chen[c], Qian Chen[c], Ivan Miguel De Cachinho Cordeiro[d])

a, Department of Building Environment and Energy Engineering, The Hong Kong Polytechnic University, Hong Kong, China

b, School of Emergency Management & Safety Engineering, China University of Mining & Technology (Beijing), Beijing, 100083, China

c, Department of Architecture and Civil Engineering, City University of Hong Kong, Hong Kong, China

d, School of Mechanical and Manufacturing Engineering, University of New South Wales, Sydney, NSW 2052, Australia

[1] Tian Chang and Anthony Chun Yin Yuen contributed equally to this work (co-first author).

Abstract: A biomass fire suppression gel foam (FSGF) with outstanding thermal stability and fire resistance performance was synthesised to improve the flame retardancy of foam agents on liquid fuel fires. The foam comprehensive index, microstructure, thermal stability, fire resistance and extinguishing properties of the FSGF were benchmarked against aqueous film-forming foam (AFFF). Subsequently, reactive forcefield (ReaxFF) molecular dynamics (MD) simulations were performed on the FSGF to study the thermokinetic properties. Based on the experimental results, a porosity layer was found on the external film of FSGF, which enhanced the thermal stability of the foam. The gelling mechanism of the foam is the formation of an O–Ca–O bond. Through MD simulations it was discovered that the remained calcium oxide/hydroxide species when deposited on fuel surfaces would promote char formation as they capture H/O atoms via dehydration. Alternatively, the foam showed better thermal stability than that of AFFF due to a lower weight loss rate and longer collapse time. The extinguishing performance tests demonstrated that the fire extinguishing time and resistance time of FSGF respectively are 72 s and 801 s,

showing a significant potential to suppress the re-ignition of tank fires.

Keywords: Gel foam, Liquid fuel fires, Thermal stability, Fire suppression, ReaxFF, Molecular Dynamics

32 **Nomenclature**

t_α	the expansion time of foam
t_β	the collapse time of foam layer where the thermocouple is located

33 **Acronyms**

AES	sodium alcohol ether sulphate
AFFF	aqueous film forming foam
EDS	energy dispersive spectrum
FCI	foam comprehensive index
FIRS	Far-infrared radiation system
FSGF	fire suppression gel foam
FTIR	Fourier transform infrared spectroscopy
MD	molecular dynamics
ReaxFF	reactive forcefield
SEM	scanning electron microscopy
TGA	thermogravimetric analysis
XPS	X-ray photoelectron spectrometry

34 # 1. Introduction

35 Liquid fuels including crude oil and petroleum refined products continue to be one
36 of the major sources of energy generation in our society while playing a significant role
37 in today's world economy. At present, large-scale crude oil storage tanks still exist
38 everywhere around the world readily to support our infrastructure and transportation
39 systems demands [1,2]. Inevitably, such storage tanks pose massive fire risks as they
40 carry large weights of fire load during a fire outbreak, which can potentially cost
41 immense economy and casualties at any time [3,4]. For instance, a crude storage tank
42 fire occurred in Cuba in August 2022, it took about six days to suppress the fire due to
43 strong flame flux radiation and a large burning area, leading to the loss of 40 % of
44 Cuba's fuel reserves [5]. To date, the AFFF is considered one of the most efficient
45 extinguishing agents for tank fires because of its good spreading performance on liquid
46 fuel surfaces [6,7]. Nevertheless, the drainage and coalescence rate of AFFF is rapidly
47 exposed to strong flame radiation due to poor fire resistance and thermal stability, which
48 may result in the re-ignition of tank fires [8]. Meanwhile, the toxic fluorocarbon

surfactants consist in AFFF pose a great threat to the environment and firefighters [9,10]. Therefore, it is essential to develop good thermal stability, fire resistance and environmental-friendly extinguishing agents to control liquid fuel fires and suppress the associated re-ignition risks.

To enhance the comprehensive performance of foaming agents, functional particles were incorporated into foaming agent chemical compounds in recent years. This includes nanoparticles [11,12], and polymers [13-15]. For example, Qiao et al. developed a microcapsule-based inhibitory foam with sodium dodecyl sulfate and found that the expansion ratio and half-life of the foam can reach up to 14 and 123 min respectively [16]. Ou et al. developed a foaming agent utilising carbon nanotubes and xanthan gum and found that the maximum initial foam height and 25 % drainage time can reach 192 mL and 347 s respectively [17]. Meanwhile, gel-based foams were developed to enhance the foam's comprehensive performance [18-21]. Xi and Shi synthesised a high-water-retaining gel foam with microbial polysaccharide, galactomannan biopolymer and organic boron complex. The half-life of the gel foam can reach up to 121.8 h, and the expansion ratio of the foam is 5.8 [22]. Zhao et al. developed a double-crosslinked gel foam for inhibiting coal spontaneous combustion and found that the half-life of gel foam can be enlarged from 1 day to 45 days [23]. Although the gel system can significantly enlarge the half-life of foam, the flow performance of foam is inhibited due to the high density of gel particles. The poor flow properties of foam will limit the dispersion when depositing on the liquid fuel surface. Therefore, it is essential to develop a foaming agent with a lofty half-life and enhanced fluidic properties such as diffusiveness and dispersioness.

The thermal stability of foaming agents is one of the key performance indicators to validate its comprehensive performance, which has been studied by some researchers in recent years [24-27]. Fan et al. prepared a compound gel foam and investigated the weight loss rate of foam via TGA. They found that the maximum weight loss rate of the coal could be decreased by 7.55% [28]. The team led by Shi (2022) synthesised a

77 gel-stabilised foam and investigated the collapse time of the gel foam. They found that
78 the gel foam could exist stably within 30 mins under a coal-burning furnace [29]. Apart
79 from that, the fire resistance capacity of foam is also used to evaluate its comprehensive
80 performance [24,30]. Zhao et al. synthesised an inorganic gel foam to suppress liquid
81 tank fires and analysed the fire resistance time of the foam. The results indicate that the
82 maximin fire resistance time of the foam can reach 485 s [31]. Qiu et al. prepared a
83 thermo-responsive fluorine-free foam and found that the fire resistance time of the foam
84 can reach about 1200 s, while the foam showed a long extinguishing time of 102 s [32].
85 However, most of these studies focus on the weight loss rate and fire resistance time of
86 gel foams, whereas studies on the collapse mechanism of gel foams are still very limited.
87 Moreover, it is hard to validate the collapse time of foam utilising an unstable heat
88 source (i.e., coal-burning furnace).
89 Although experimental approaches provided direct performance indication of the
90 effectiveness of the foaming agents, the comprehensive fire suppression mechanisms
91 and the chemical process are yet to be fully revealed. With recent advancements in
92 reactive forcefields (ReaxFF) molecular dynamics (MD) simulations to study the
93 thermodegradation of polymers, this may present further insights into foam agent fire
94 suppression thermokinetics phenomena [33, 34]. The use of ReaxFF-MD was recently
95 found to be an effective way to reveal chemical reaction pathways that lead to fire
96 reduction mechanisms [35-37]. For instance, Cordeiro et al. demonstrated the atomic
97 level thermal degradation behaviour of flame retarded High-density polyethylene via
98 ReaxFF-MD simulation and found that the double/triple C–C bond favoured the
99 pyrolysis behaviour of the flame retarded polymers in the early degradation stage [38].
100 Xu et al. investigated the pyrolysis mechanisms of epoxy resin polymers by combining
101 experiments and ReaxFF-MD simulation and illustrated the detailed formation paths of
102 typical pyrolysis products, like H_2, H_2O, CO and CH_4 [39].
103 To address the missing knowledge in the field, this paper aims to develop a biomass
104 FSGF with good thermal stability and spreading performance for liquid tank fires. The

sodium alcohol ether sulphate and hydrolysed protein were selected as the compounding foaming agent, which was then used with sunflower pectin as the gelling agent and calcium lactate as the crosslinking agent to prepare the FSGF. It is important to note that a stable heating source which is provided by a Far-infrared radiation system was developed to analyse the thermal stability of foams. The comprehensive value, microstructure, gelling mechanism and charring mechanism of the FSGF were analysed systematically. Moreover, the fire extinguishing and fire resistance performance of FSGF was evaluated compared with AFFF. Furthermore, MD simulations were conducted to strengthen the understanding of the molecular breakdown process of the FSGF and its elevated chemical compounds and species during the process to identify the in-depth fire suppression mechanisms.

2. Materials and methods

2.1 Materials

Sodium alcohol ether sulphate (AES, batch number: S11101115; Mw=106.12 g/mol; 70% purity) and calcium lactate ($C_6H_{10}CaO_6 \cdot 5H_2O$; Batch number: I92501115; Mw=308.3 g/mol; 99% purity) were offered by Shandong Ecosol Chemical Technology Co., Ltd. Hydrolysed protein (Total nitrogen: 14.5%; Ash: 6.1%; Moisture: 6%; 90% purity) was supplied by Shijiazhuang Xuermei Biotech Co., Ltd. Sunflower pectin (Batch number: 689730128; Average Mw is 187371 g/mol and it is quantified by America Agilent PL-GPC220. The detaild tests prosedures and results are shown in the supplementary material; DE: 60.81; GalA: 95.63 %; Ash ≤1; 99% purity) was offered by Qingdao Haiweisen Biotechnology Co., Ltd. Besides, a commercial AFFF (Surface tension: 16.1mN/m; Expansion ratio: 7.5; half-life: 5.4 min) with 6% active matter content (Fluorocarbon surfactants #1212; Hydrocarbon surfactants #FCHJ-50) was also used, supplied by Hunan Xuan Fire Technology Co., Ltd.

2.2 Synthesis and optimisation of FSGF

As shown in Fig. 1a, 20 mL compounding foaming agent (The ratio of AES/ hydrolysed protein is 2:8) and 20 mL sunflower pectin solutions were first poured into

a container to stir 90 s with a rate of 3000 r/min and then 10 mL calcium lactate solution was sprayed to the container stirring 30 s. Finally, the FSGF was synthesised based on the laboratory scale. To obtain the optimal formation of FSGF, the FCI was introduced by Zhang et al. [40] to evaluate the comprehensive properties of foam and can be expressed as:

$$FCI = \frac{3}{4}\frac{V_2}{V_1}T_{1/2} \quad (1)$$

Where V_2/V_1 means the foam expansion ratio and $T_{1/2}$ is the half-life of foam. The Waring Blender method was used to determine the foam expansion ratio. In the experiments, the initial total volume of foam solution was 50 mL (V_1). Subsequently, the prepared foam was poured into a graduated cylinder to record the foaming volume (V_2) and half-life ($T_{1/2}$). Half-life is defined as the time for the foam to separate out half of the foam solution and is commonly used to estimate foam stability [41].

2.3 Experiment methods

The bench performance tests were used to characterize the microstructure, gelling mechanism and thermal stability of foams, as shown in Fig. 1b. The scanning electron microscopy (SEM) integrated with energy dispersive spectroscopy (EDS) was used to observe the morphology of foams and to analyse the elemental composition and distribution. Fourier transform infrared spectroscopy (FTIR) and X-ray photoelectron spectrometry (XPS) were served to analyse the typical bond structure and gelling mechanism of foams. The weight loss rate, thickness change and internal temperature of foam were investigated via thermogravimetric analysis (TGA) and far-infrared radiation system (FIRS). After that, a customised gel-foam fire extinguishing system was developed to test the spreading and fire resistance performances of foams. The detailed test procedures are shown in the supplementary material.

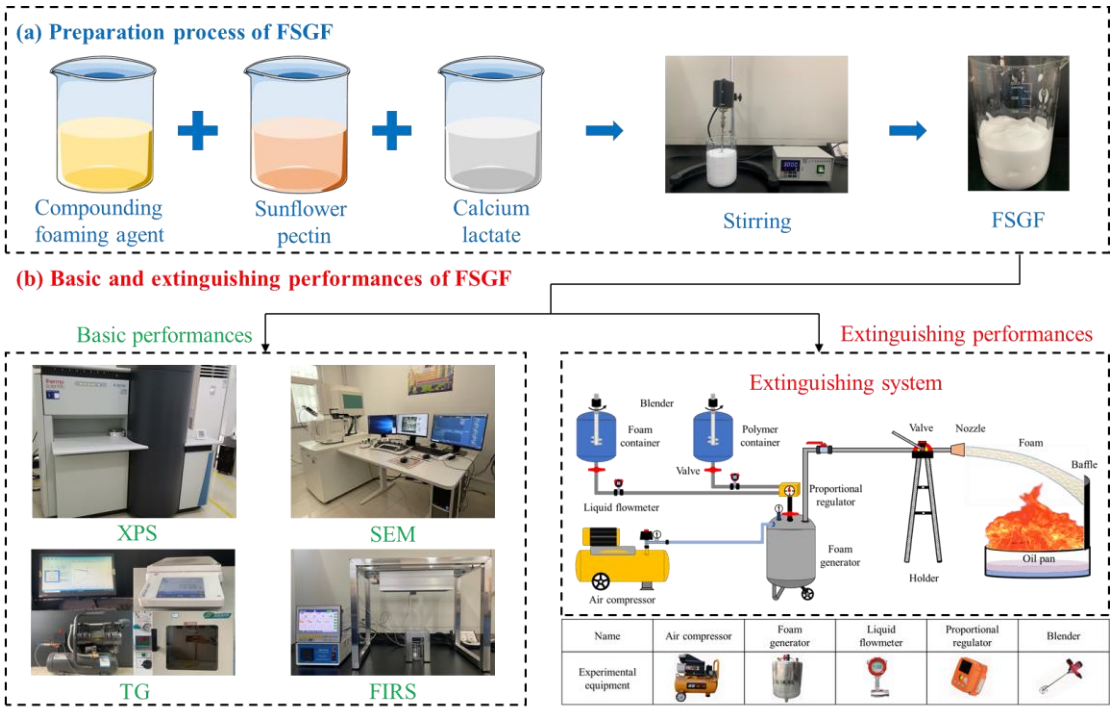

Fig. 1 Foam preparation process, benchmark and extinguishing performance tests conducted in this study.

2.4 Molecular modelling

The numerical model of calcium pectin (the fibric gel structure in FSGF) was developed via the Amsterdam Modelling Suite (AMS) [42]. The ReaxFF parameters for the H/C/O/Ca systems to build and optimize the model were based on Hong's study [43]. The initial step of the MD model began with the construction of a monomer unit of calcium pectin, D-Galacturonic acid, as shown in Fig. 2a. Subsequently, the monomer was populated to a long D-Galacturonic acid chain (n=20). Afterwards, a single calcium pectin chain was formed by the crosslinking of two D-Galacturonic acid chains and 10 calcium ions, as shown in Fig. 2b. Moreover, five calcium pectin chains were generated in a 70 Å × 70 Å × 70 Å simulation box. The initial computational domain was compressed via the MD deformation module to achieve a targeted cell of 32 Å × 32 Å × 32 Å in a period of 500 ps, as shown in Fig. 2c. The final geometry corresponds to a density of 1.8 g/cm^3, which resembles with the theoretical density of calcium pectin. Moreover, a stable periodic cell was obtained after a system relaxed under constant pressure and temperature (NPT) conditions [44]. After that, the z

dimension of the periodic cell is then extended to 70 Å to obtain a domain of 32 Å x 32 Å x 70 Å. To characterize the charring and oxidation process of FSGF, 1400 oxygen molecules was filled into the periodic cell via PACKMOL [45]. Ultimately, the periodic cell was heated from 300 K to 2500, 3000 and 3500 K respectively in a period of 100 ps to analyse the pyrolytical performances of FSGF. The detailed chemical reaction pathway of FSGF was analysed via the ChemTraYzer module in AMS [46].

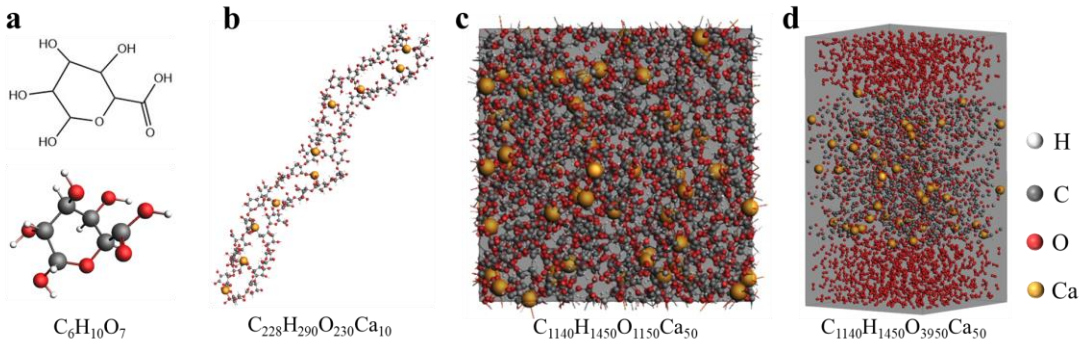

Fig. 2 (a) D-Galacturonic acid, (b) Single chain of calcium pectin, (c) The molecular geometry of Calcium pectin, (d) Snapshot of calcium pectin filled with oxygen in a periodic box.

3. Results and discussions

3.1 Optimisation of FSGF formulation

3.1.1 Single factor analysis

The compounding foaming agent with a concentration of 0.5 wt% shows a high FCI according to our previous studies [47]. Thus, different contents of sunflower pectin were added to 0.5 wt% compounding foaming agent solution for stirring and foaming to get the optimal sunflower pectin concentration. The foam expansion ratio, half-life and FCI of compound foaming agents with different mass fractions of sunflower pectin are shown in Fig. 3a. It can be seen that the foam expansion ratio decreases upon increasing sunflower pectin. This can be attributed to the fact that the polymer will increase the surface tension of the foam solution [48]. While the half-life increases upon increasing sunflower pectin. This phenomenon can be explained by the fact that the polymer can decrease the liquid drainage rate of foam [49]. Meanwhile, the FCI increases significantly with the mass fraction of sunflower pectin until it reaches its

maximum value at a mass fraction of 0.8 wt% (i.e., the optimal concentration). Based on the results, the sunflower pectin with a total mass fraction of 0.8 wt% was chosen for the development of the FSGF with calcium lactate.

Different contents of calcium lactate were added to the solution with 0.5 wt% compounding foaming agent and 0.8 wt% sunflower pectin solution for stirring and foaming to select the optimal calcium lactate concentration. The foam expansion ratio, half-life and FCI of compound foaming agents with different mass fractions of calcium lactate were shown in Fig. 3b. It can be obtained that the FCI increases initially with the mass fraction of calcium lactate, followed by a decrease trend. When the mass fraction was 0.05 wt%, the crosslinking reaction was not completely carried out due to a low concentration of calcium lactate. As the mass fraction increased to 0.10 wt%, the FCI climbed to the highest value. This can be attributed to the calcium lactate and sunflower pectin reacting completely to form a continuous gel skeleton at the end of stirring time. With more calcium lactate added to the sunflower pectin solution, the half-life of the foam decreased. This is because the gel skeleton was stirred into fragments due to the gel skeleton was formed before the end of stirring time.

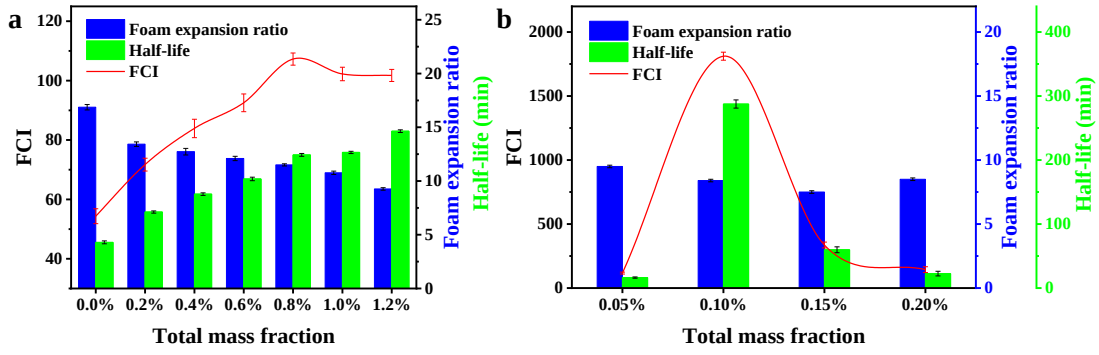

Fig. 3 The FCI of compounding foaming agent with different mass fractions of sunflower pectin (a) and calcium lactate (b).

3.1.2 Orthogonal analysis

Based on the single-factor experimental results, a three-factor and three-level orthogonal experiment was carried out, including the foam expansion ratio and half-life as the key evaluation indices. The factors in the orthogonal experiment included the

compounding foaming agent (A), sunflower pectin (B) and calcium lactate (C). The level of each factor is shown in Table 1, and the experimental results are shown in Table 3. Ki (i = 1,2,3) is the mean value of the experimental data of each factor at the ith level. R is the range, which indicates the extent of the experimental change of the factor within the value range.

Table 1 Test factors and level coding table

Level	Factor		
	A/wt%	B/wt%	C/wt%
1	0.4	0.6	0.05
2	0.5	0.8	0.10
3	0.6	1.0	0.15

As despised in Table 2, it can be observed that factor C shows a significant influence on R_2 with 206.22 compared with that of factors A and B. Meanwhile, the maximum mean value of factor C is K_2 (255.39). Thus, 0.10 wt% (level 2) is selected as the optimal concentration of calcium lactate. Besides, it can be seen that factor B shows the greatest influence on R_1 with 2.60, followed by factor A. The foam expansion ratio decreases upon increasing sunflower pectin, but considering the half-life of foam, the optimal addition concentration of sunflower pectin is 0.8 wt% (level 2). Moreover, the foam expansion ratio increases initially with factor A, followed by a decrease trend. Thus, 0.5 wt% (level 2) is selected as the optimal concentration of the compound foaming agent. In conclusion, the optimal formulation of FSGF is composed of 0.5 wt% compounding foaming agent, 0.8 wt% sunflower pectin and 0.1 wt% calcium lactate. The average foam expansion ratio (E), half-life and FCI of FSGF are 8.40, 287.50 min and 1811.04 according to sample 10 to 12, respectively.

Table 2 Orthogonal test and experimental results

Sample	Factor A (wt%)	Factor B (wt%)	Factor C (wt%)	E	$T_{1/2}$ (min)
1	1(0.40)	1(0.60)	1(0.05)	7.60	10.95
2	1(0.40)	2(0.80)	2(0.10)	6.40	268.77
3	1(0.40)	3(1.00)	3(0.15)	5.40	49.87
4	2(0.50)	1(0.60)	2(0.10)	9.60	186.87

5	2(0.50)	2(0.80)	3(0.15)	7.60	58.17
6	2(0.50)	3(1.00)	1(0.05)	6.80	228.62
7	3(0.60)	1(0.60)	3(0.15)	9.20	39.47
8	3(0.60)	2(0.80)	1(0.05)	8.00	20.13
9	3(0.60)	3(1.00)	2(0.10)	6.40	310.53
10	2(0.50)	2(0.80)	2(0.10)	8.40	293.07
11	2(0.50)	2(0.80)	2(0.10)	8.30	288.97
12	2(0.50)	2(0.80)	2(0.10)	8.50	280.47
K_1	6.46	8.80	7.47		
K_2	8.00	7.20	7.47		
K_3	7.87	6.20	7.27		
R_1	1.54	2.60	0.20		
K_1	109.86	79.10	86.57		
K_2	151.89	115.69	255.39		
K_3	123.38	196.34	49.17		
R_2	42.03	117.33	206.22		

To investigate the role of the sunflower pectin and calcium lactate in gelling reaction, SEM and FTIR of the aqueous foam and polymer foam were analysed and compared with that of the FSGF. Detailed information on different foam formulas is shown in Table 3.

Table 3 Detailed information on foam formulas

Foaming solution	Compounding foaming agent (wt%)	Sunflower pectin (wt%)	Calcium lactate (wt%)
Aqueous foam	0.5	0.00	0.00
Polymer foam	0.5	0.80	0.00
FSGF	0.5	0.80	0.10

3.2 Microscope structure and gelling mechanism

3.2.1 SEM analysis

To characterise the microscope structure of FSGF, the SEM-EDS images of polymer foam and FSGF were investigated, as shown in Fig. 4. It can be observed that the film structure of polymer foam shows an entire and smoother surface, as shown in Fig. 4a, indicating sufficient stability of the polymer foam. This is because a continuous film can suppress the diffusion of air inside the film [50]. However, apart from the

continuous surface, it can be seen that many pores grew at the surface of FSGF. This can be ascribed to the fact that the sunflower pectin was cross-linked with calcium lactate. Moreover, the porose structure was incorporated to improve the thermal stability of foam [51].

Fig. 4c exhibits the distribution features of key elements on the film surface of FSGF. It can be observed that all of the elements are distributed on the film surface uniformly, indicating a stable cross-linking reaction rate. The total mass fraction of the elements of O and C is about 80 %, indicating that the domestic composite of FSGF is an organic composite. These two elements are mainly derived from sunflower pectin and hydrolysed protein, both of which are environmentally friendly. The element of Ca originated from calcium lactate, while elements of N are from the amino group in hydrolysed protein and a minor number of elements of Na and S are from AES.

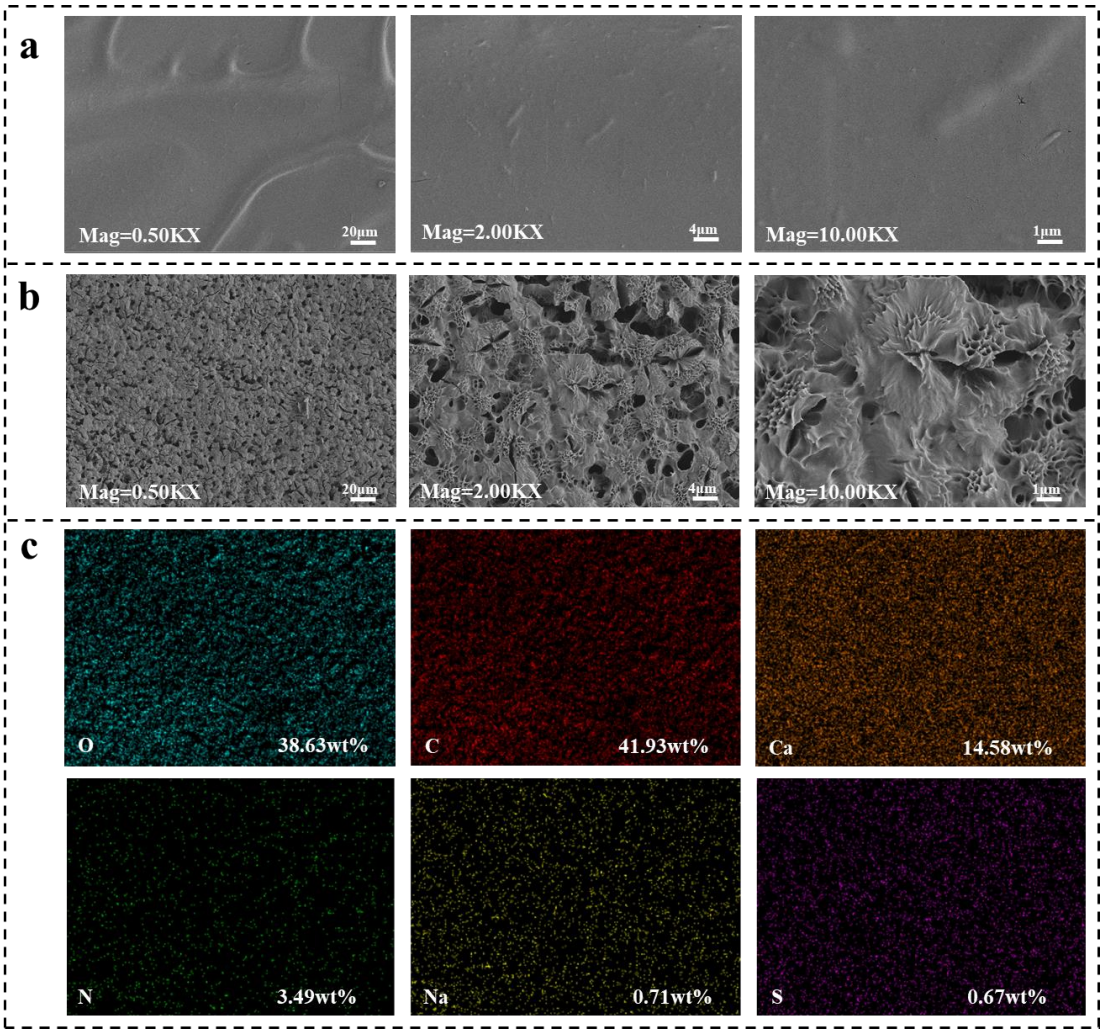

Fig. 4 (a) SEM images of the polymer foam; (b) SEM images of the FSGF; (c) Surface EDS of film structure in FSGF.

3.2.2 FTIR-XPS analysis

Fig. 5a shows the FTIR spectra of the aqueous foam, polymer foam and FSGF. The peak at 3300 cm^{-1} is attributed to N–H stretching vibration [52], and those at 3426 cm^{-1} to O–H stretching vibration [53]. These peaks are the characteristic absorption peaks in the functional groups of AES, hydrolysed protein and sunflower pectin, respectively. Compared with the aqueous foam, the peak at 3426 cm^{-1} is the superposition of stretching vibration of O–H from sunflower pectin and N–H from hydrolysed protein, so the strength is increased [54]. Compared with the polymer foam, the symmetrical stretching vibration absorption peak of the $–COO^-$ bond shifts from 1656 to 1639 cm^{-1} and the asymmetrical stretching vibration absorption peak of the $–COO^-$ bond from 1430 to 1452 cm^{-1}, indicating that the crosslinking reaction occurred with the introduction of calcium lactate [55].

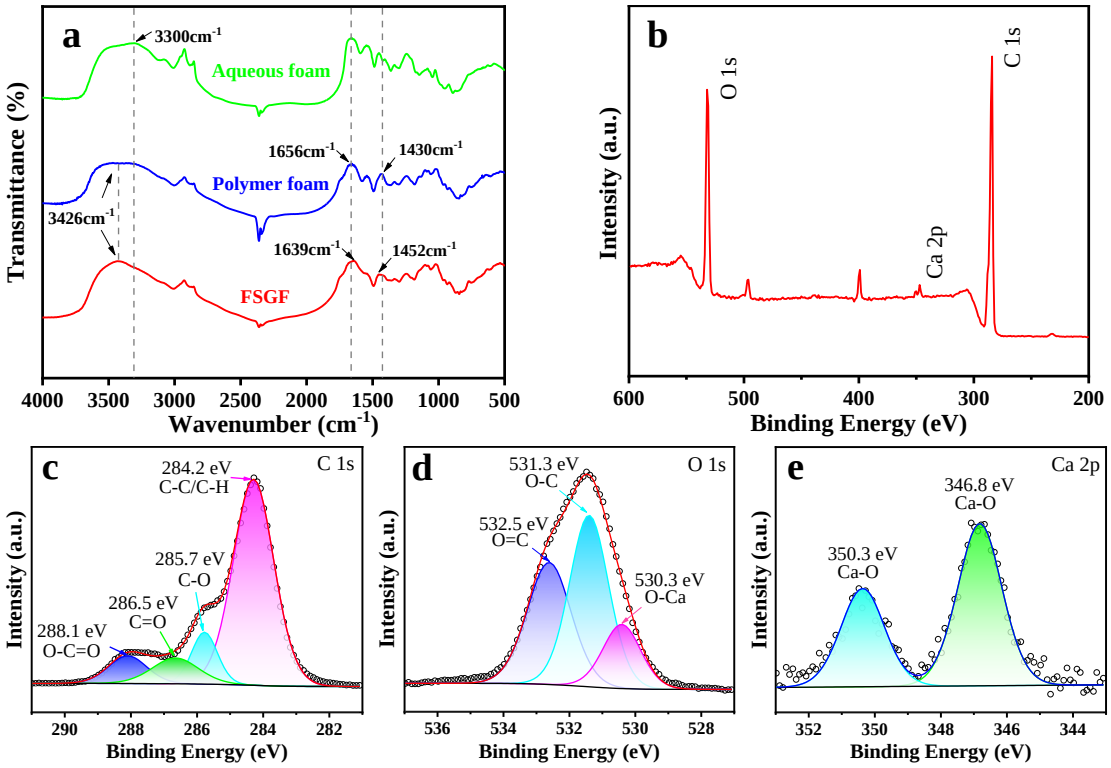

Fig. 5 (a) FTIR spectra of aqueous foam, polymer foam and FSGF; (b) Full scan XPS spectra and high-resolution XPS spectra for (c) C1s, (d) O1s and (e) Ca 2p of the FSGF.

To strengthen the understanding of the porose structure of FSGF and crosslinking interactions between sunflower pectin and calcium lactate. The XPS data of FSGF was

analysed, as shown in Fig. 5b. Fig. 5c shows the C 1 s XPS data, which can be divided into four binding energies: C–C/C–H (284.2 eV), C–O/C–N (285.7 eV), C=O (287.5 eV), and O–C=O (288.1 eV) in sunflower pectin and calcium lactate [56,57]. The C–C/C–H bonds correspond to stronger binding energy, accounting for 66.4%, while the C–O/C–N, C=O and O–C=O bonds correspond to weaker binding energy, accounting for 16.6 %, 8.1 % and 8.9%, respectively. In the high-resolution O 1s XPS spectrum (Fig. 5d), the peaks observed at 531.3 eV and 532.3 eV correspond to the groups of O–C and O=C [58]. Furthermore, the peak at 530.3 eV is derived from the O–Ca of the porose structure [59]. As shown by the Ca 2 p XPS data (Fig. 5e), the characteristic peaks of Ca–O 2p3/2 and Ca–O 2p1/2 were observed at 346.8 eV and 350.3 eV [60], which confirmed the presence of Ca element on the film surface of FSGF due to the cross-linking of sunflower pectin and calcium lactate.

3.2.3 Gelling mechanism and film structure

Fig. 6 shows the gelling mechanism and film structural diagram of FSGF. Based on the analysis of FTIR and XPS, it can be known that the gelling mechanism of FSGF is due to the formation of the O–Ca–O bond. As shown in Fig.6a, the first reaction pathway is the ionization of sunflower pectin and calcium lactate. The sunflower pectin ionizes –COO^- bond. Meanwhile, the calcium lactate releases Ca^{2+}. Subsequently, the –COO^- bond cross-linked with Ca^{2+} to generate the O–Ca–O bond leading to a porose three-dimensional gel network, as shown in Fig. 6b.

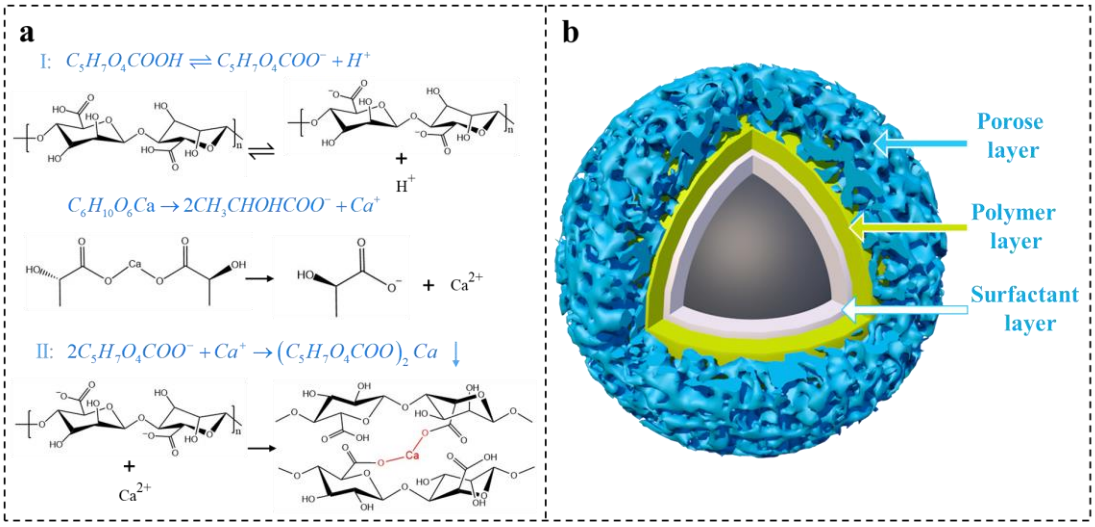

Fig.6 The gelling mechanism (a) and schematic diagram of film structure (b) for FSGF.

To clarify the film structure of FSGF clearly, a 3D schematic of the foam was carried out via Cinema 4D software, as shown in Fig. 6b. It can be seen that the internal layer of the film is the compound foaming surfactants (i.e., AES and hydrolysed protein), which forms the bench bubble structure of FSGF. The middle layer of the film is attached by a polymer with high viscosity (i.e., sunflower pectin). It can block the diffusion of gas to enhance the stability of foam. In the external layer, the film is covered by fibric structure which is built according to the SEM results. The porose layer can prevent the bubble from flame radiation to decrease the collapse process.

3.3 Thermal stability and thermokinetic analyses

3.3.1 Thermogravimetric

The TG curves of AFFF and FSGF are shown in Fig. 7a. It can be observed that the 100 % water loss temperature of AFFF is about 150 °C, while that of FSGF is up to 164 °C, indicating that the FSGF shows a well water retention performance. To quantify the weight loss rate of different foams, the DTG curves of AFFF and FSGF are figured out, as shown in Fig. 7b. It can be seen that the weight loss rate of FSGF is lower than that of AFFF over the period. The maximum weight loss rate of FSGF is about 48 %/min, whereas that of AFFF is up to 59 %/min. This is mainly because the porose networks can decrease the collapse rate of foam to enhance the thermal stability of foam.

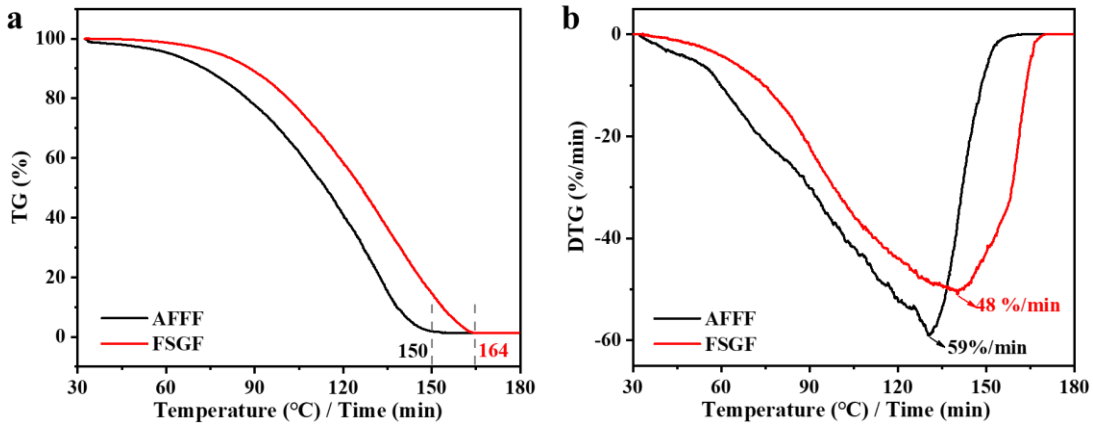

Fig. 7 TG (a) and DTG (b) curve of AFFF and FSGF.

3.3.2 Thermal stability

To strengthen the understanding of analysing the thermal stability of foam, the collapse process of foams exposed to a radiation heating source is investigated. Fig. 8a, 8b and 8c respectively exhibit the typical collapse images and thickness changes of FSGF, polymer foam and AFFF. It can be found that the thickness of foams increased initially. This is because the expansion of foam size is led by gas expansion under high temperatures. After that, the thickness of the foam gradually decreases due to the coarsening and coalescence of the foam film. Besides, it is worth noting that a charring layer was formed for FSGF. The layer can block the thermal radiation to slow down the collapse rate of FSGF [61]. On top of that, it can be noticed that the collapse time of AFFF is about 1200 s, while that of FSGF is more than 1800 s. This phenomenon indicates that the FSGF show well thermal stability. Meanwhile, the thickness of polymer foam collapsed to 2 cm approximately after 1800 s, whereas that of FSGF remains about 6 cm, highlighting the porose structure of FSGF as shown in Fig. 6b. This demonstrates that FSGF enhances the thermal stability of foam film, which is advantageous for fire resistance performances.

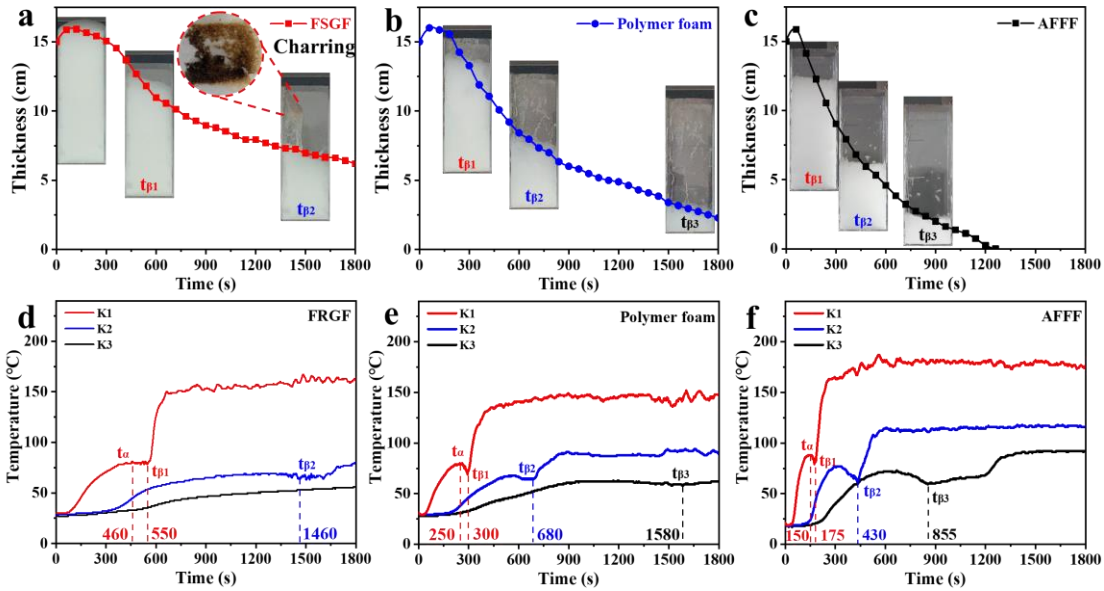

Fig. 8 Changes of the foam thickness exposed to radiation: (a) FSGF, (b) Polymer foam, (c) AFFF; Internal temperature of foams at different depths: (d) FSGF, (e) Polymer foam, (f) AFFF.

Apart from that, the internal temperature distribution of foams is analysed. Fig. 8d,

8e and 8f respectively show the internal temperature of FSGF, polymer foam and AFFF at different depths. It can be observed that the temperature line of foams can be divided into three stages: steady increase (before t_α, t_α means the expansion time of foam), slight decrease (between t_α and t_β, t_β means the collapse time of the foam layer where the thermocouple is located) and remarkable climb (after t_β). In the steady increase period, the internal temperature of foams increases owing to exposure to thermal radiation. Besides, the foam thickness increased at the same time. The t_α of FSGF, polymer foam and AFFF are 460, 250 and 150 s, respectively. In the slight decrease stage, the temperature of the foam layer declined. Because the water evaporation will take much heat away [62]. However, the temperature of the FSGF layer nearly keeps a stable value in this period. This phenomenon can be ascribed to the fact that the charring layer attached to K1 disturbed the detection of temperature. Moreover, the $t_{\beta 1}$ of FSGF, polymer foam and AFFF are 550, 300 and 175 s, respectively, indicating that the FSGF displays better thermal stability than other foams. In the remarkable climb stage, the temperature of the foam layer shows a dramatic rise because the thermocouples are exposed to the radiation heating source.

3.3.3 Thermokinetic analysis

To demonstrate the detailed pyrolysis and charring process of FSGF, the thermokinetics of the FSGF were analysed via ReaxFF-MD simulation. The main gaseous pyrolysis products of FSGF are H_2O and CO_2. As shown in Fig. 9a, it can be seen that the number of H_2O molecules increased initially and then kept a stable value during the entire pyrolysis period. Moreover, the maximin number of H_2O molecules is about 570 when pyrolysed at 2500 k, accounting for 78.6 % of the total H atoms in the raw calcium pectin polymers. Apart from that, it can be observed that the maximin number of CO_2 molecules can reach up to 180 at 3500 k, accounting for 15.8 % of the total C atoms in the raw calcium pectin, as shown in Fig.9b. The generation of H_2O and CO_2 were advantages for enhancing the extinguishing efficiency of foam, because the evaporation can decrease the temperature of the flame area and the CO_2 suppressed the

combustion of liquid fuel.

Meanwhile, some typical products can be found in char, such as CaO and $Ca(OH)_2$. The evolution of $Ca(OH)_2$ during the pyrolysis period is shown in Fig.9c. It can be observed that the number of $Ca(OH)_2$ shows a fluctuating trend. This is because the chemical property of $Ca(OH)_2$ was unstable, which could react with other components in the periodic cell. The detailed formation paths of $Ca(OH)_2$ are displayed in Fig.9d. It is known that the Ca atoms were oxidated to CaO initially after a breakdown from the crosslinked structure of calcium pectin. After that, the CaO was translated to $Ca(OH)_2$ due to reacting with H_2O. Both CaO and $Ca(OH)_2$ are good charring agents as they absorb H and O atoms via dehydration effects to promote the formation of char. [63,64].

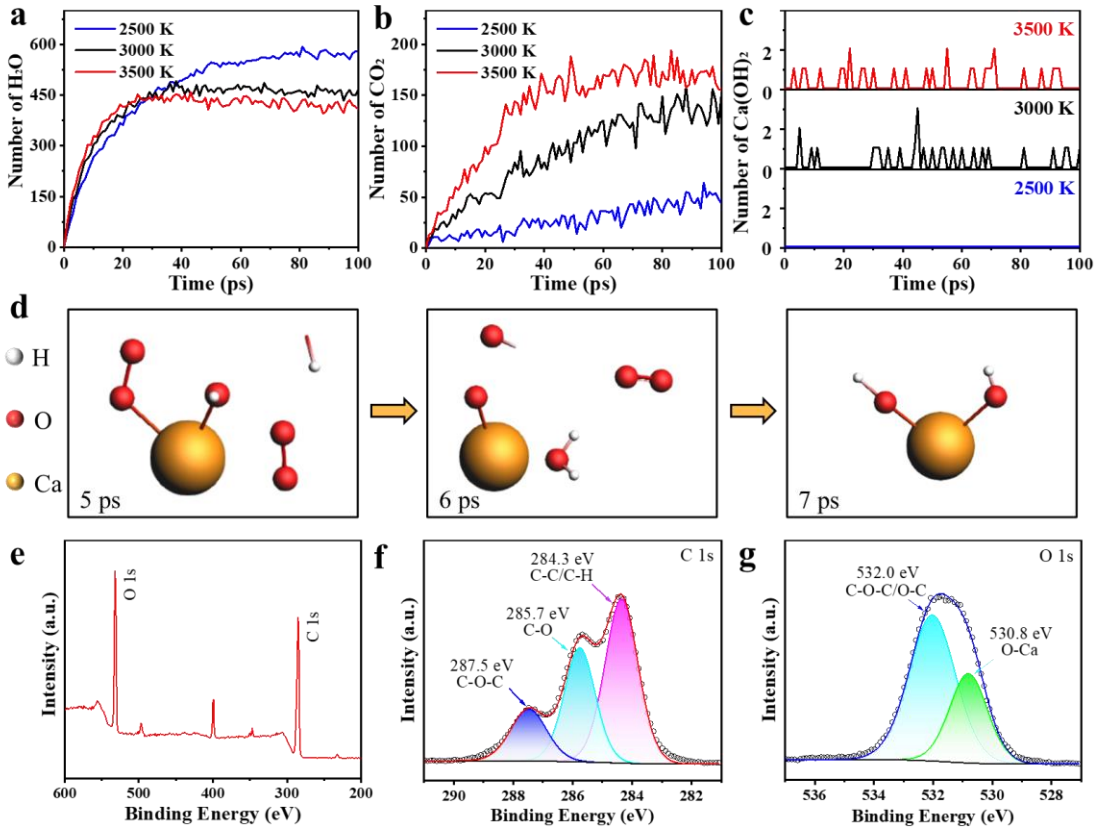

Fig. 9 Evolution of H_2O (a), CO_2 (b) and $Ca(OH)_2$ (c) during the pyrolysis of FSGF; (d) The formation paths of $Ca(OH)_2$ during the pyrolysis of FSGF; (e) Full scan XPS spectra and high-resolution XPS spectra for (f) C1s and (g) O1s of the char residues from FSGF.

To validate the MD results, XPS tests were served to study the dehydration effects of the CaO and $Ca(OH)_2$ produced by FSGF. Fig. 9e displays the full scan XPS spectra of

two main elements including C and O in char residues from FSGF. Compared with the XPS spectra of FSGF without charring in Fig. 5c and Fig. 5d, a different functional group, C–O–C, can be found at the high-resolution XPS spectra of C1s in Fig. f, which appeared at 287.5 eV [65]. Meanwhile, it also appeared at 530.0 eV at the high-resolution XPS spectra of O1s in Fig. 9g [66]. This indicated that the hydroxyl on calcium pectin chains dehydrated with each other [67,68]. The phenomenon proved the charring mechanism of FSGF obtained from MD simulation. Therefore, it can be concluded that the MD simulation demonstrated a valid description of the pyrolysis mechanisms of FSGF in water vapour generation and char layer protection.

3.4 Fire extinguishing and resistance performance

3.4.1 Fire extinguishing capacity

Fig. 10a and 10b respectively show the typical images of FSGF and polymer foam in the fire suppression process. The spreading efficiency of AFFF is similar to FSGF, so the results are not included here for brevity. It can be observed that the extinguishing efficiency of FSGF is higher than that of polymer foam over the period. For instance, FSGF covered approximately half of the burning area at 40 s, while polymer foam just accumulated a small foam layer near the injection point. At 60 s, the FSGF almost extinguished the pool fire and there was just a small ball of flame, whereas the polymer foam still suppressed the edge fire of the pan. Ultimately, the fire was extinguished by FSGF at 72 s, a 17 s decrease from the extinguishing time of polymer foam.

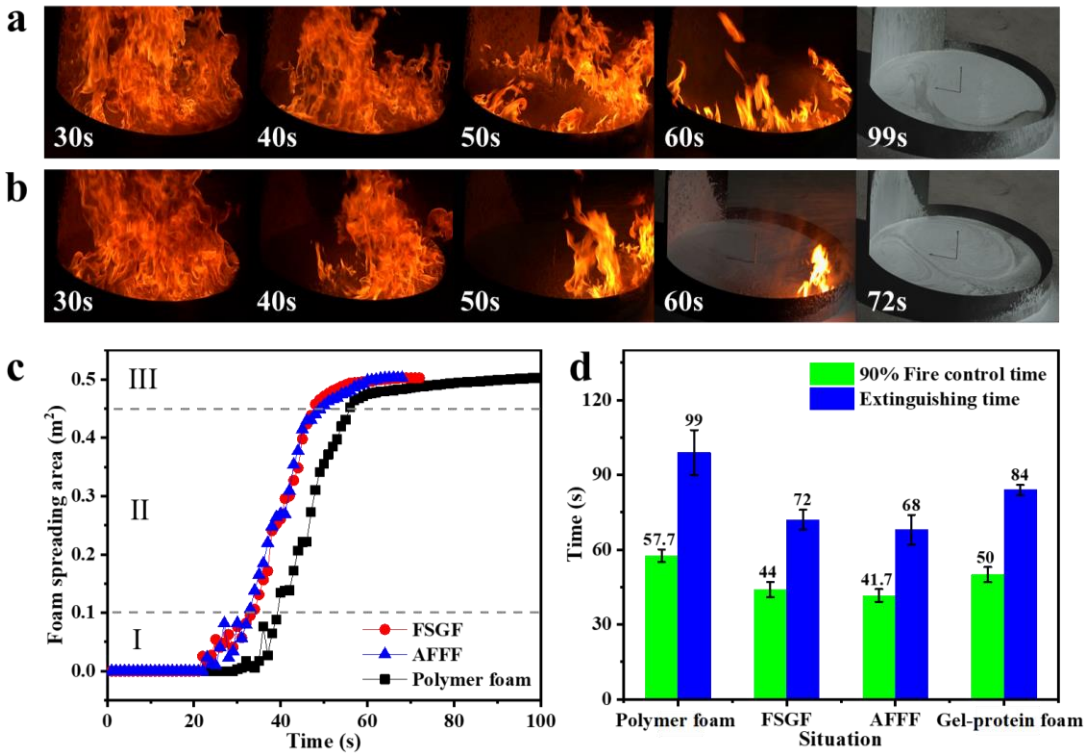

411

412 Fig. 10 The fire extinguishing process of different types of foam: (a) polymer foam, (b) FSGF;

413 the foam spreading area (c) and extinguishing time (d) of foams.

414 To strengthen the understanding of foam spreading performance, the foam spreading

415 area was figured out, as shown in Fig. 10c. It can be observed that the spreading process

416 of foams can be divided into three periods: fluctuating rise (I), stable climb (II) and

417 slight increase (III). In stage I, the foam spreading area shows a fluctuating increase

418 trend due to the foam breaking down pretty fast when it went through the flame field

419 with high radiation [79]. In stage II, it rises gradually due to the formation of the foam

420 layer with the continuous injection of a foaming agent. It can be found that the initial

421 time of stable spread (i.e., the time when the foam spreading area is equal to 0.1 m^2) for

422 FSGF is about 30 s, while that of polymer foam is up to 40 s approximately. This is

423 because FSGF can accumulate faster than polymer foam near the injection point due to

424 the unique porose networks, which can enhance the thermal stability of foam based on

425 the results from Fig. 8. The foam spreading area ascends slowly in stage III, that is

426 because lots of foam was consumed to suppress the burning area of pan edge where is

427 far away from the injection point, as shown the image at 60 s in Fig. 10a.

Meanwhile, the fire extinguishing time of different types of foam was analysed to illustrate the spreading efficiency of foams, as shown in Fig. 10d. It can be seen that the extinguishing time of FSGF is 72 s, a 27 s decrease from that of polymer foam. This is mainly due to its better thermal stability. It is worth noting that the extinguishing time of FSGF also should be lower than that of AFFF due to better thermal stability, while it just shows a close value of 68 s for AFFF. This phenomenon can be ascribed to the fact that the AFFF with a high foam expansion ratio can narrow its shortage in thermal stability in foam spreading performance tests [70]. Besides, FSGF shows a superior spreading efficiency against gel-protein foam (a foam which was synthesised in our previous work). This can be ascribed to the fact that FSGF shows a stronger film structure. According to Fig. 5b, it is known that the film of FSGF consists of a surfactant layer, polymer layer and porose layer, whereas that of gel-protein foam is just made of a surfactant layer and gel layer [47].

3.4.2 Fire resistance performance

Fig. 11a and 11b respectively show the typical images of AFFF and FSGF in the fire resistance period. It can be observed that the FSGF display a better fire resistance performance compared with AFFF over the period. For example, at 300 s, there was burning outside the edge of the ignition tank for AFFF, whereas the FSGF was still stably covered on the fuel surface. At 400 s, the AFFF collapsed gradually and the fuel surface near the ignition tank was boiling with fire. While the FSGF just broke down along the edge of the ignition tank. Besides, a charring circle can be found outside the flame area, which corresponded to the results from thermal stability tests according to Fig. 8a. Afterwards, the fire suddenly turned violent due to the complete breakdown of AFFF after 50 s, while the FSGF was still efficiently made the fire under control at the same time. Meanwhile, it is speculated that the collapse mechanism of AFFF is layer by layer based on the observed boiling phenomenon and the appearance of violent fire. However, the collapse path of FSGF can be seen as circle by circle due to the thermo-isolation effect of the charring layer. In this way, the charring layer can decrease the

collapse process to improve the fire resistance of foam.

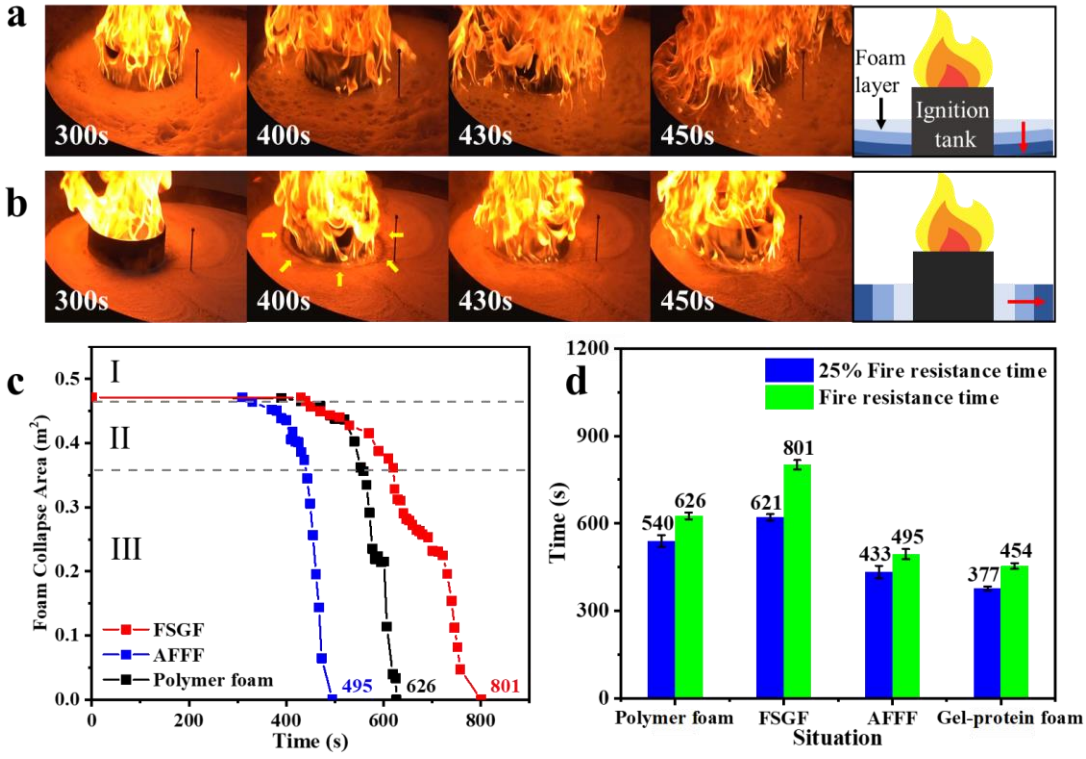

Fig. 11 The fire resistance process of different types of foam: (a) AFFF, (b) FSGF; the foam collapse area (c) and fire resistance time (d) of foams.

To further analyse the fire resistance of foams, the foam collapse area and fire resistance time of foams were recorded, as shown in Fig. 11c and 11d, respectively. It can be observed that the foam collapse area kept a stable value in stage I due to the stable coverage of the foam layer. Subsequently, it gradually decreased in stage II because the foam collapsed layer by layer or circle by circle. Ultimately, it dramatically dropped with the expansion of the burning area in stage III. Meanwhile, it can be seen that the FSGF shows the highest fire resistance time with 801 s, a 28 % and 62 % increase over that of polymer foam and AFFF, respectively. This can be ascribed to the prevention of the charring layer. Besides, the fire resistance time of FSGF shows a 76 % increase against that of gel-protein foam due to the porose film structure. It can be summarized that the FSGF shows a good fire resistance performance, which will be conducive to suppressing the re-ignition of large-scale tank fires.

4. Conclusions

In this work, a novel biomass FSGF was developed to improve the fire suppression efficiency of liquid fuel fires. Benchmarking fire suppression performances of the foam including comprehensive index, microscope structure, gelling mechanism, thermal stability, charring mechanism and extinguishing performances were systemically analysed. The major findings of this study were broken down into fourfold including (i) FSGF shows the optimal FCI with 0.5 wt% compound foaming agent, 0.8 wt% sunflower pectin and 0.1 wt% calcium lactate after orthogonal analysis. And the foam expansion ratio, half-life and FCI of the FSGF are 8.40, 287.50 min and 1811.04, respectively; (ii) The gelling mechanism of the foam is the crosslinking of $–COO^-$ ionised from sunflower pectin cross-linking with Ca^{2+} released from calcium lactate to from the O–Ca–O bond, which leads to the generation of a porose layer attached to the film of FSGF. The layer can improve the thermal stability of foam by preventing thermal radiation. (iii) The fastest weight loss rate of the foam is about 48 %/min, lower than that of AFFF with 59 %/min. Moreover, the MD results revealed that the proposed FSGF promoted char formation as it acted as a dehydration agent to absorb H and O atoms, leaving behind carbonation bonds favourable to forming char. (iv) The extinguishing time of the FSGF is 72 s, a 27 s decrease from that of polymer foam. Meanwhile, the fire resistance time of the foam is up to 801 s, a 62 % increase over that of AFFF, highlighting that the FSGF shows a significant fire extinguishing efficiency.

Overall, the FSPF shows a porose film structure, outstanding comprehensive index, excellent thermal stability and fire resistance capacity, which will play a pivotal role in suppressing the re-ignition of tank fires. Although the scenarios considered in this work are similar to those in a real fire scenario, the performance of FSGF needs to be further estimated in large-scale tank fires.

Credit author statement

Chang Tian: Conceptualization, Data curation, Formal analysis, Methodology,

Investigation, Validation, Visualization, Writing-original draft. Anthony Chun Yin Yuen: Resources, Supervision, Project administration, Funding acquisition, Review & editing. Jinlong Zhao: Resources, Supervision, Project administration, Funding acquisition. Timothy Bo Yuan Chen, Qian Chen, Ivan Miguel De Cachinho Cordeiro: Software, Validation, Methodology, Review & editing.

Acknowledges

This study was sponsored by the PolyU UGC funding (P0044994). Also, it is funded by the National Natural Science Foundation of China (No. U2333210), the China Postdoctoral Science Foundation (No. 2023M733282) and the Fundamental Research Funds for the Central Universities (No. 2023JCCXAQ05).

References

[1] D.L. Zou, J.G. Sun, H. Wu, Y.F. Hao, Z. Wang, L.F. Cui. Experimental and numerical studies on the impact resistance of large-scale liquefied natural gas (LNG) storage outer tank against the accidental missile. Thin-Walled Struct., 158(2021), Article 107189.

[2] Z. Wang, K. Hu, Y. Zhao. Distribution characteristics and simplified model of external explosion loading on large-scale doom-roof steel tanks. Structures, (2024), Article 106150.

[3] J. Lei, W. Deng, S. Mao, Y. Tao, H. Wu, C. Xie. Flame geometric characteristics of large-scale pool fires under controlled wind conditions. Proc. Combust. Inst., 39(2023), pp. 4021-4029.

[4] X. Wang, B. Li, B. Han, X. Jin, D. Zhang, M. Bi. Explosion of high pressure hydrogen tank in fire: Mechanism, criterion, and consequence assessment. J. Energy Storage, 72(2023), Article 108455.

[5] J. Yang, B. Zhang, L. Chen, X. Diao, Y. Hu, G. Suo, R. Li, Q. Wang, J. Li, J. Zhang, Z. Dou. Improved solid radiation model for thermal response in large crude oil tanks. Energy, 284(2023), Article 128572.

[6] S. L. Giles, A. W. Snow, K. M. Hinnant, R. Ananth. Modulation of fluorocarbon

surfactant diffusion with diethylene glycol butyl ether for improved foam characteristics and fire suppression. Colloid Surf. A-Physicochem. Eng. Asp., 579(2019), Article 123660.

[7] X. Jia, Y. Luo, R. Huang, H. Bo, Q. Liu, X. Zhu. Spreading kinetics of fluorocarbon surfactants on several liquid fuels surfaces. Colloid Surf. A-Physicochem. Eng. Asp., 589(2020), Article 124441.

[8] R. Zhou, X. Lang, X. Zhang, B. Tao, L. He. Thermal stability and insulation characteristics of three-phase fire-fighting foam exposed to radiant heating. Process Saf. Environ. Protect., 146(2021), pp. 360-368.

[9] C. Abril, J.L. Santos, J. Martin, I. Aparicio, E. Alonso. Occurrence, fate and environmental risk of anionic surfactants, bisphenol A, perfluorinated compounds and personal care products in sludge stabilisation treatments. Sci. Total Environ., 711(2020), Article 135048.

[10] P.F. Yan, S. Dong, K.D. Pennell, N.L. Capiro. A review of the occurrence and microbial transformation of per-and polyfluoroalkyl substances (PFAS) in aqueous film-forming foams (AFFFs)-impacted environments. Sci. Total Environ., 10(2024), Article 171883.

[11] C. Liu, G. Zhu, C. Chen, X. Guo, C. An, J. Ding. Research on the fire-extinguishing effectiveness of a new nano-scale aerogel fire-extinguishing agent. Therm. Sci. Eng. Prog., 37(2023), Article 101625.

[12] Y. Sheng, C. Yan, Y. Peng, Y. Li, L. Ma, Q. Wang, W. Gao, S. Zhang. Influence of nano-aluminum hydroxide on foam properties of the mixtures of hydrocarbon and fluorocarbon surfactants. J. Mol. Liq., 357(2022), Article 119158.

[13] D. Bilanovic, J. Starosvetsky, R.H. Armon. Preparation of biodegradable xanthan–glycerol hydrogel, foam, film, aerogel and xerogel at room temperature. Carbohydr. Polym., 148(2016), 243-250.

[14] J. Zhu, N. Zheng, Z. Yang, X. Li, T. Lei. Experimental study on the foam-stabilising advantages and foam stabilisation mechanism of novel microbial

polysaccharides. J. Mol. Liq., 385(2023), Article 122428.
[15] Y. Yang, X. Wu, J. Zhang, F. Shang, F. Xiao, K. Li, X. Liu. Plateau boundary blocking effect of Nano-SiO2 on foam properties of Gemini fluorocarbon and hydrocarbon surfactant mixed solution. Fire Saf. J., 142(2024), Article 104019.
[16] J. Qiao, D. Zhao, Y.Y. Zhao, W. Lu, M.M. Li, X.M. Hu, Y.T. Liang, F.C. Tian, S. Ju, B.R. Yan. Preparation and characteristics of sustained-release microcapsule-based inhibitory foam with high foaming ratio. Fuel, 302(2021), Article 121219.
[17] H. Ou, H. Cao, S. Wang, Z. Min, H. Xue, H. Bi, J. Wang. Study on the effects of carbon nanotubes and xanthan gum on the performance of hydrocarbon surfactant foam systems. J. Loss Prev. Process Ind., 87(2024), Article 105243.
[18] L. Ma, X. Fan, G. Wei, Y. Sheng, S. Liu, X. Liu. Preparation and characterisation of antioxidant gel foam for preventing coal spontaneous combustion. Fuel, 338(2023), Article 127270.
[19] L. Zhang, Y. Xie, L. Li. Fabrication of poly (vinyl alcohol) foam/gel composite used for cold storage by combing molding foaming and freeze-thawing technologies. Polym. Test., 131(2024), Article 108350.
[20] C. Han, S. Nie, Z. Liu, S. Liu, H. Zhang, J. Li, H. Zhang, Z. Wang. A novel biomass sodium alginate gel foam to inhibit the spontaneous combustion of coal. Fuel, 314(2022), Article 122779.
[21] K. Zhou, L. Yin, K. Gong, Q. Wu. 3D Vascular-structured Flame-retardant Cellulose-based photothermal aerogel for Solar-driven interfacial evaporation and wastewater purification. Chem. Eng. J., 464(2023), Article 142616.
[22] X. Xi, Q. Shi. Study of the preparation and extinguishment characteristic of the novel high-water-retaining foam for controlling spontaneous combustion of coal. Fuel, 288(2021), Article 119354.
[23] W. Zhao, L. Ma, Z. Wang, F. Wang, L. Zhang, H. Ma, W. Wang. Preparation and characterisation of highly stable double-crosslinked gel foam for inhibiting coal spontaneous combustion. Colloid Surf. A-Physicochem. Eng. Asp., 685(2024),

584 Article 133179.
585 [24] T.M. Nguyen-Ha, T.B. Nguyen, T.A. Nguyen, L.H. Pham, D.H. Nguyen, D.M.
586 Nguyen, D. Hoang, E. Oh, J. Suhr. Novel high-performance sustainable
587 polyurethane nanocomposite foams: Fire resistance, thermal stability, thermal
588 conductivity, and mechanical properties. Chem. Eng. J., 474(2023), Article 145585.
589 [25] M. Wu, G. Yu, W. Chen, S. Dong, Y. Wang, C. Liu, B. Li. A pulp foam with highly
590 improved physical strength, fire-resistance and antibiosis by incorporation of
591 chitosan and CPAM. Carbohydr. Polym., 278(2022), Article 118963.
592 [26] M. Wu, Y. Liang, Y. Zhao, W. Wang, X. Hu, F. Tian, Z. He, Y. Li, T. Liu.
593 Preparation of new gel foam and evaluation of its fire extinguishing performance.
594 Colloid Surf. A-Physicochem. Eng. Asp., 629 (2021), Article 127443.
595 [27] K. Zhou, K. Gong, C. Wang, M. Zhou, J. Xiao. Construction of Ti3C2 MXene
596 based fire resistance nanocoating on flexible polyurethane foam for highly efficient
597 photothermal conversion and solar water desalination. J. Colloid Interface Sci.,
598 630(2023), pp. 343-354.
599 [28] X.L. Fan, L. Ma, Y.J. Sheng, X.X. Liu, G.M. Wei, S.M. Liu. Experimental
600 investigation on the characteristics of XG/GG/HPAM gel foam and prevention of
601 coal spontaneous combustion. Energy, 284(2023), Article 128710.
602 [29] Q. Shi, B. Qin, Y. Xu, M. Hao, X. Shao, H. Zhuo. Experimental investigation of
603 the drainage characteristic and stability mechanism of gel-stabilised foam used to
604 extinguish coal fire. Fuel, 313(2022), Article 122685.
605 [30] X. Yu, N. Jiang, X. Miao, F. Li, J. Wang, R. Zong, S. Lu. Comparative studies on
606 foam stability, oil-film interaction and fire extinguishing performance for fluorine-
607 free and fluorinated foams. Process Saf. Environ. Protect., 133(2020), pp. 201-215.
608 [31] J. Zhao, J. Yang, Z. Hu, R. Kang, J. Zhang. Development of an environmentally
609 friendly gel foam and assessment of its thermal stability and fire suppression
610 properties in liquid pool fires. Colloid Surf. A-Physicochem. Eng. Asp., 692(2024),
611 Article 133990.

612 [32] K. Qiu, X. Yu, Q. Li, H. Li, N. Kang, S. Lu. Thermo-responsive fluorine-free foam
613 stabilised by PEO-PPO-PEO triblock copolymer (EO) 100 (PO) 65 (EO) 100 for
614 pool fire suppression. SmartMat(2023), pp. e1232.
615 [33] A.C.Y. Yuen, T.B.Y. Chen, I.M.D.C. Cordero, H. Liu, A. Li, W. Yang, S.C.P.
616 Cheung, Q.N. Chan, S. Kook, G.H. Yeoh. Developing a solid decomposition
617 kinetics extraction framework for detailed chemistry pyrolysis and combustion
618 modelling of building polymer composites. J. Anal. Appl. Pyrolysis, 163(2022),
619 Article 105500.
620 [34] A.C.Y. Yuen, T.B.Y. Chen, C. Wang, W. Wei, I. Kabir, J.B. Vargas, Q.N. Chan, S.
621 Kook, G.H. Yeoh. Utilising genetic algorithm to optimise pyrolysis kinetics for fire
622 modelling and characterisation of chitosan/graphene oxide polyurethane
623 composites. Compos. Part B Eng., 182(2020), Article 107619.
624 [34] A.C.Y. Yuen, G.H. Yeoh, V. Timchenko, T. Barber. LES and multi-step chemical
625 reaction in compartment fires. Numer. Heat Tranf. A-Appl., 68(2015), pp. 711-736.
626 [36] C. Sun, A. Zhu, R. Wang, H. Liu. Pyrolysis reaction mechanisms and chlorine
627 migration of tetrachlorobiphenyl a through the integration of ReaxFF-MD and DFT.
628 J. Environ. Chem. Eng., 12(2024), Article 112778.
629 [37] J. Wang, G. Li, Z. Zhang, Q. Huang, B. Niu, Y. Zhang, D. Long. Detailed insights
630 of polydimethylsiloxane (PDMS) degradation mechanism via ReaxFF MD and
631 experiments. Chem. Eng. J., 488(2024), Article 150728.
632 [38] I.M.D.C. Cordero, T.B.Y. Chen, A.C.Y. Yuen, Q. Chen, W. Yang , C. Wang, W.
633 Wang, Q.N. Chan, J. Zhang, W. Yang, G.H. Yeoh. Characterising flame-retardant
634 mechanism of phosphorous-containing intumescent coating on polyethylene via
635 ReaxFF MD simulations. Chem. Eng. J., 480(2024), Article 148169.
636 [39] M.X. Xu, J.Y. Di, Y.C. Wu, X.X. Meng, H. Jiang, J.H. Li, Q. Lu. Insights into the
637 pyrolysis mechanisms of epoxy resin polymers based on the combination of
638 experiments and ReaxFF-MD simulation. Chem. Eng. J., 473(2023), Article
639 145404.

[40] C. Zhang, P. Wang, G. Song. Study on enhanced oil recovery by multi-component foam flooding. J. Pet. Sci. Eng., 177(2019), pp. 181-187.

[41] S. Ju, Q. Huang, G. Wang, J. Li, E. Wang, C. Qin, J. Qiao. Rheological and morphological characteristics of foam fluid using hydroxypropyl guar and surfactant. J. Pet. Sci. Eng., 211(2022), Article 110124.

[42] AMS 2021.1. SCM, Theoretical Chemistry, Vrije Universiteit, Amsterdam, The Netherlands (2021). Available: http://www.scm.com.

[43] D. Hong, Z. Cao, X. Guo. Effect of calcium on the secondary reactions of tar from Zhundong coal pyrolysis: A molecular dynamics simulation using ReaxFF. J. Anal. Appl. Pyrolysis, 137 (2019), pp. 246-252.

[44] D. Hofmann, L. Fritz, J. Ulbrich, C. Schepers, M. Bohning. Detailed-atomistic molecular modeling of small molecule diffusion and solution processes in polymeric membrane materials. Macromol. Theory Simul., 9(2000), pp. 293-327.

[45] L. Martinez, R. Andrade, E.G. Birgin, J.M. Martinez. PACKMOL: A package for building initial configurations for molecular dynamics simulations. J. Comput. Chem., 30(2009), pp. 2157-2164.

[46] S. Arvelos, O. Abrahao Jr, C.E. Hori. ReaxFF molecular dynamics study on the pyrolysis process of cyclohexanone. J. Anal. Appl. Pyrolysis, 141(2019), Article 104620.

[47] C. Tian, J. Zhao, J. Yang, J. Zhang, R. Yang. Preparation and characterisation of fire-extinguishing efficiency of novel gel-protein foam for liquid pool fires. Energy, 263(2023), Article 125949.

[48] R. Gou, W. Pu, Y. Liu, R. Liu, Y. Chen, T. Zhang, X. Du. Unlocking the enormous potential of biological materials: Polymer-assisted foam for enhanced oil recovery in fractured porous media. J. Mol. Liq., 403(2024)., Article 124808.

[49] C. Li, A. Wu, Z. Zhao. Effect of sodium alginate and polyvinyl alcohol polymers on the foaming performance of dodecyl dimethyl betaine solutions. Colloid Surf. A-Physicochem. Eng. Asp., 676(2023), Article 132151.

668 [50] Q. Guo, W. Ren, J. Zhu, J. Shi. Study on the composition and structure of foamed
669 gel for fire prevention and extinguishing in coal mines. Process Saf. Environ.
670 Protect., 128(2019), pp. 176-183.
671 [51] D. Liu, W. Xia, J. Liu, X. Wang, J. Xue. Ultrasound-assisted alkali extraction of
672 RG-I enriched pectin from thinned young apples: Structural characterisation and
673 gelling properties. Food Hydrocolloids, 151(2024), Article 109879.
674 [52] Z. NBian, Y. Li, H. Sun, M. Shi, Y. Zheng, H. Liu, C. Liu, C. Shen. Transparent,
675 intrinsically stretchable cellulose nanofiber-mediated conductive hydrogel for
676 strain and humidity sensing. Carbohydr. Polym., 301(2023), Article 120300.
677 [53] Y. Zheng, Q. Li, B. Lin, Y. Zhou, Q. Liu, G. Zhang, Y. Zhao. Real-time analysis of
678 the changing trends of functional groups and corresponding gas generated law
679 during coal spontaneous combustion. Fuel Process. Technol., 199(2020), Article
680 106237.
681 [54] S. Li, G. Zhou, Y. Wang, B. Jing, Y. Qu. Synthesis and characteristics of fire
682 extinguishing gel with high water absorption for coal mines. Process Saf. Environ.
683 Protect., 125(2019), pp. 207-218.
684 [55] Q. Wang, L. Zhang, Y. Liu, G. Zhang, P. Zhu. Characterisation and functional
685 assessment of alginate fibers prepared by metal-calcium ion complex coagulation
686 bath. Carbohydr. Polym., 232(2020), Article 115693.
687 [56] L.H. Grey, H.Y. Nie, M.C. Biesinger. Defining the nature of adventitious carbon
688 and improving its merit as a charge correction reference for XPS. Appl. Surf. Sci.,
689 653(2024), Article 159319.
690 [57] L. Cheng, R. Ghobeira, P. Cools, Z. Liu, K. Yan, N. De Geyter, R. Morent.
691 Comparative study of different nitrogen-containing plasma modifications applied
692 on 3D porous PCL scaffolds and 2D PCL films. Appl. Surf. Sci., 516 (2020), Article
693 146067.
694 [58] Y. Yao, D. Zhou, Y. Shen, H. Wu, H. Wang. Highly transparent, writable and
695 photoluminescent foldable polymer film: When fluorescent dyes or pigments join

696 cellulose-based microgel. Carbohydr. Polym., 263(2021), Article 117977.
697 [59] C.V. Flores, J.L. Obeso, H. Viltres, E. Torres-Garcia, A.R. Rajabzadeh, S.
698 Srinivasan, R.A. Peralta, I.A. Ibarra, C. Leyva. Spent coffee ground–calcium
699 alginate biosorbent for adsorptive removal of methylene blue from aqueous
700 solutions. RSC Sustainability, 2(2024), pp. 239-246.
701 [60] N. Zhang, H. Xue, R. Hu. The activity and stability of CeO 2@ CaO catalysts for
702 the production of biodiesel. RSC advances, 8(2018), pp. 32922-32929.
703 [61] X. Hu, Z. Sun. A method for calculating thermal resistance of the intumescent char
704 layer of fired ultra-thin fire-retardant coating. Int. Commun. Heat Mass Transfer,
705 121(2021), Article 105126.
706 [62] D. Ma, L. Pang, Y. Zhang. Experimental study on low pressure heat transfer
707 properties of water evaporator with screen separation element. Int. J. Therm. Sci.,
708 193(2023), Article 108492.
709 [63] X.L. Li, F.H. Zhang, R.K. Jian, Y.F. Ai, J.L. Ma, G.J. Hui, D.Y. Wang. Influence
710 of eco-friendly calcium gluconate on the intumescent flame-retardant epoxy resin:
711 Flame retardancy, smoke suppression and mechanical properties. Composites,
712 Part B, 176(2019), Article 107200.
713 [64] Y.A. Criado, M. Alonso, J.C. Abanades. Kinetics of the CaO/Ca(OH)2
714 hydration/dehydration reaction for thermochemical energy storage applications.
715 Ind. Eng. Chem. Res., 53(2014), pp. 12594-12601.
716 [65] L. Sun, L. Ding, X. Guo, Y. Wang, X. Liu, Y. Ren, Y. Li. “One for two” strategy to
717 construct an organic-inorganic polymer colloid for flame-retardant modification of
718 flax fabric and rigid polyurethane foam. Int. J. Biol. Macromol., 275(2024), Article
719 133562.
720 [66] Y. Ding, Z. Chen, C. Tang, W. Huang, X. Ren, K. Zhou, H. Hu. Development of a
721 pyrolysis reaction model for epoxy based flame retardant composites: Relationship
722 between pyrolysis behavior and material composition. Chem. Eng. J., 495(2024),
723 Article 153628.

[67] W. Cai, Z. Li, J. Liu, S. Qiu, Y. Pan, Z. Xu, C. Ma, Y. Hu. Recyclable and removable functionalization based on Diels-Alder reaction of black phosphorous nanosheets and its dehydration carbonization in fire safety improvement of polymer composites. Composites, Part A, 140(2021), Article 106157.

[68] K. Gong, H. Huang, C. Shi, X. Qian, L. Yin, K. Zhou. In-situ encapsulated MXene nanosheets with bimetallic phosphate: towards for reducing the fire risk of epoxy composites. Composites, Part A, 174(2023), Article 107731.

[69] Z. Wang, X. Jiang, C. Yang, B. Zhou. Experimental study on thermal stability and burn-back performance of aqueous film forming foam agent (AFFF) with short-chain fluorocarbon surfactant or flame retardant. Fire Saf. J., 146(2024), Article 104135.

[70] M. Lou, H. Jia, Z. Lin, D. Zeng, J. Huo. Study on fire extinguishing performance of different foam extinguishing agents in diesel pool fire. Results Eng., 17(2023), Article 100874.

Declaration of Interest Statement

The authors declare that they have no known competing financial interests or personal relationships that could have appeared to influence the work reported in this paper.